Topology in Electronic and Magnetic Materials as a Function of Crystalline Properties

Maia G. Vergniory[#], Claudia Felser[##], Iñigo Robredo, Kartik Samantha, Jonathan Noky and Jorge Cardenas-Gamboa

Topology and crystalline symmetries are fundamental concepts in condensed matter physics. They have garnered significant interest, particularly in the study of materials with exotic electronic properties. The interplay between topology and crystalline symmetries leads to a rich variety of phenomena and new classes of materials. In our group, we have investigated this interplay in both electronic and magnetic materials, first through an extensive high-throughput search, and then by analyzing the topological properties of the selected materials in more detail. We have widely studied nodal lines, Weyl crossings, and the chiral properties of spin and orbital angular momentum, as well as superconductivity. We have also started to develop a new formalism to include topological correlations in Green's functions. Finally, we analyzed the charge density waves in kagome systems.

In the following, we present the results of our high-throughput search of topological materials and our studies on nodal lines and Weyl points in double perovskites and the spin texture of chiral semimetals.

High-throughput searches at any filling of electronic and phononic materials

High-throughput computations have shown that many more materials are topological than was initially thought. We expanded this approach to include all processable entries in the Inorganic Crystal Structure Database and studied the band structures of materials both at and away from the Fermi energy. Almost 88% of these materials exhibit at least one topological band [1].

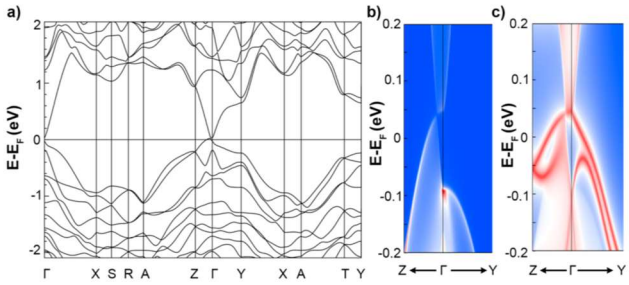

Fig. 1: Electronic band structure of KMg_4Bi_3 with uniform lattice expansion of 3.5% along all axes.

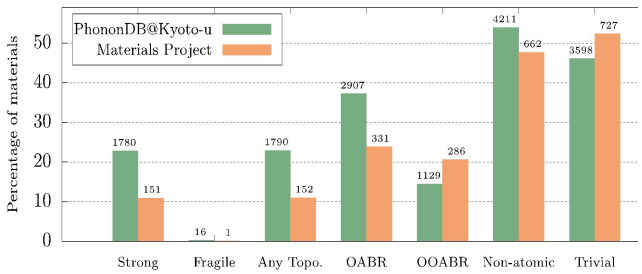

Fig. 2: Statistics of nontrivial phonon band sets for the phonon materials from PhononDB@Kyoto-u (green) and Materials Project (orange) databases.

In addition to the electronic structure, the phonon band structure can also display nontrivial topology. Our searches identified KMg_4Bi_3 as a new narrow-bandgap semiconductor. We grew it experimentally and characterized it by ARPES. It undergoes a topological transition at certain pressures (Figure 1) [2].

We also conducted a high-throughput computational screening of more than 10,000 two-phonon materials. We found nontrivial phonon bands in more than half of the studied materials and identified approximately 1000 as promising for experimental investigation (Figure 2) [3]. The robustness of topological surface phonon states means they can be used for frequency filtering or mechanical energy attenuation under imperfect conditions, as well as for heat transfer and infrared photoelectronics.

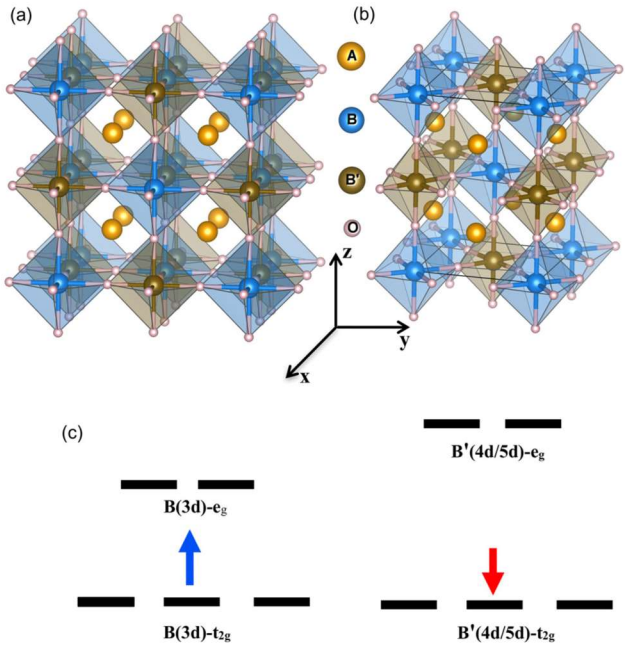

Fig. 3: Crystal structure and schematic energy level diagram of rocksalt-ordered double perovskites $A_2BB'O_6$.

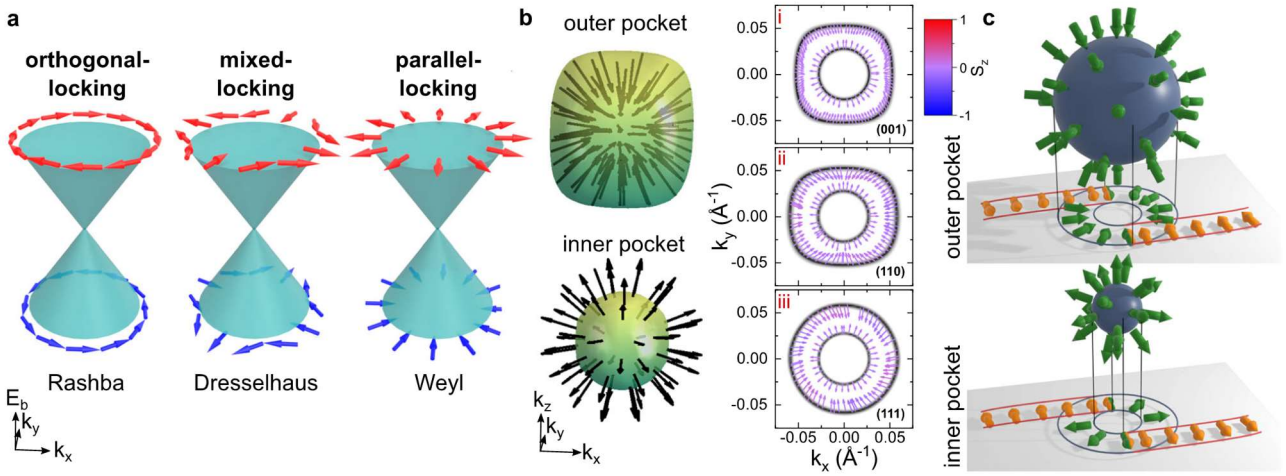

Fig. 4: Overview of prototypical forms of spin–momentum locking with linear momentum.

Topological phonons are also promising for constructing phonon diodes and acoustic waveguides. When the time-reversal symmetry is broken, several topological effects, such as quantum anomalous or quantum valley Hall-like effects, can be realized in topological phononic materials.

3*d*–4*d*/5*d*-based oxide double perovskites

Magnetism and spin–orbit coupling are two fundamental and interconnected properties of oxide materials that can give rise to various topological transport phenomena, including the anomalous Hall and Nernst effects. These transport responses can be significantly enhanced by designing electronic structures with large Berry curvature. In this context, rocksalt-ordered double perovskites ($A_2BB'O_6$) with two distinct transition metal sites are powerful platforms for exploration and research (Figure 3). Herein, we present a comprehensive study on the intrinsic anomalous transport in cubic and tetragonal stable double perovskites with 3*d*–4*d*/5*d* elements (Table 1). Our findings reveal that certain double perovskites exhibit a large anomalous Hall effect and topological band crossings near the Fermi energy [4].

Table 1. Summary of the results of selected materials considered in this study.

Material	SG	B-3d site	B′-4d/5d site	B (μ_B)	B′ (μ_B)	M (μ_B/f.u.)	MS	AHC (S cm^{-1})	AHC$_{max}$(ΔE) (S cm^{-1})	ANC (A m^{-1} K^{-1})	ANC$_{max}$(ΔE) (A m^{-1} K^{-1})
Ba_2FeMoO_6	225	$Fe^{3+}-3d^5$	$Mo^{5-}-4d^1$	3.97	−0.40	3.99	FiM	6.94	37 (0.20)	0.04	−0.18 (0.20)
Ba_2CoMoO_6	225	$Co^{2+}-3d^7$	$Mo^{6-}-4d^0$	2.70	0.03	2.99	FM	0.00	0.00	0.00	0.00
Ba_2MnMoO_6	225	$Mn^{2+}-3d^5$	$Mo^{6-}-4d^0$	4.54	0.11	4.99	FM	0.00	0.00	0.00	0.00
Ba_2FeReO_6	225	$Fe^{3+}-3d^5$	$Re^{5+}-5d^2$	3.90	−0.92	3.06	FiM	33.43	329 (0.20)	0.04	−1.20 (0.14)
Ba_2MnReO_6	225	$Mn^{2+}-3d^5$	$Re^{6+}-5d^1$	4.52	−0.66	4.03	FiM	278	536 (0.03)	1.52	−2.10 (0.10)
Ba_2NiReO_6	225	$Ni^{2+}-3d^8$	$Re^{6+}-5d^1$	1.70	0.71	2.95	FM	−495	−571 (0.01)	0.220	2.51 (0.05)
Ba_2NiWO_6	225	$Ni^{2+}-3d^8$	$W^{6+}-5d^0$	1.71	0.06	2.01	FM	0.00	0.00	0.00	0.00
Sr_2NiMoO_6	87	$Ni^{2+}-3d^8$	$Mo^{6-}-4d^0$	1.67	0.07	2.00	FM	0.00	0.00	0.00	0.00
Sr_2FeMoO_6	87	$Fe^{3+}-3d^5$	$Mo^{5-}-4d^1$	4.06	−0.55	3.99	FiM	73.68	99 (0.17)	0.03	0.94 (0.16)
Sr_2CoOsO_6	87	$Co^{2+}-3d^7$	$Os^{6+}-5d^2$	2.68	−1.18	1.16	FiM	300	517 (0.12)	−1.61	3.13 (0.20)
Sr_2CoReO_6	87	$Co^{2+}-3d^7$	$Re^{6+}-5d^1$	2.44	−0.44	2.03	FiM	−22	200 (0.19)	−0.52	−1.97 (0.20)
Sr_2CrOsO_6	87	$Cr^{3+}-3d^3$	$Os^{5+}-5d^3$	2.74	−1.79	0.18	FiM	0.00	0.00	0.00	0.00
Sr_2NiOsO_6	87	$Ni^{2+}-3d^8$	$Os^{6+}-5d^2$	1.68	1.22	3.84	FM	176	206 (−0.08)	−0.66	−2.60 (−0.19)
Sr_2NiReO_6	87	$Ni^{2+}-3d^8$	$Re^{6+}-5d^1$	1.67	−0.65	1.03	FiM	447	447	−0.30	2.54 (0.01)

Listed are the space group (SG), charge state, and electron occupancy at the B-3d and B′-4d/5d sites, the magnetic moment at the B-3d and B′-4d/5d sites, theoretical magnetization per formula unit (f.u.), magnetic ground state (MS), AHC, maximum AHC, ANC, and maximum ANC. The maximum values are obtained in an energy window of 200 meV around the Fermi level. ΔE indicates the energy distance in eV of the maximum values with regard to the Fermi level.

Table 1: Summary of results of selected materials considered in this study.

Spin texture in chiral semimetals

Spin–orbit coupling in noncentrosymmetric crystals leads to spin–momentum locking, which is a directional relationship between the spin angular momentum and linear momentum of an electron. Although isotropic orthogonal Rashba spin–momentum locking has been studied for decades, its counterpart, isotropic parallel Weyl spin–momentum locking, has remained underexplored. Theoretically, Weyl spin–momentum locking should only be realized in structurally chiral cubic crystals in the vicinity of Kramers–Weyl or multifold fermions. We used spin- and angle-resolved photoemission spectroscopy to demonstrate the Weyl spin–momentum locking of multifold fermions in the chiral topological semimetal PtGa. We found that the electron spin of the Fermi arc surface states is orthogonal to their Fermi surface contour for momenta close

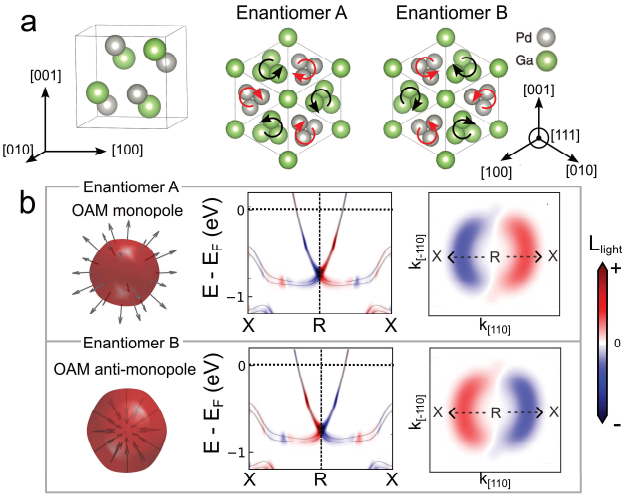

Fig. 5: Sketch of chiral crystal structure of PdGa (B20 structure), highlighting the helical winding of atoms along the [111] direction.

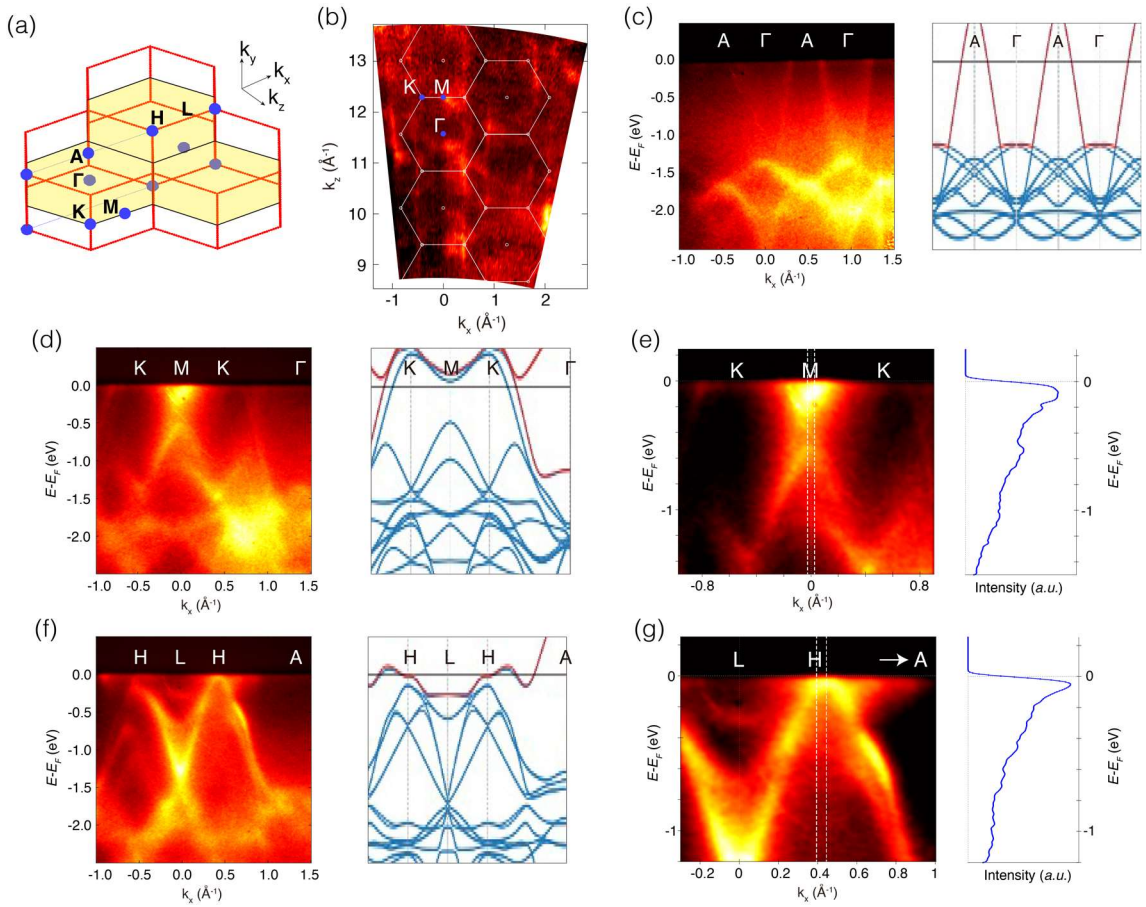

Fig. 6: (a) Bulk Brillouin zone (BZ) of $NbGe_2$ with high-symmetry A, Γ, K, M, H, and L points labeled. (b) Out-of-plane Fermi surface (FS) mapping, taken within the photon energy range of 280–700 eV. The BZ boundary is marked by white lines. (c, d, f) Photoemission intensity plots (left) and corresponding calculated band structures (right) along high-symmetry directions. The high symmetry points are labeled on the figures. (e, g) Enlarged views of (d) and (f), respectively. The density-of-states (DOS) around the M and H points, respectively, are plotted in the right-hand panels.

to the projection of the bulk multifold fermion at the Γ point, which is consistent with Weyl spin–momentum locking (Figure 4). Direct measurements of the bulk spin texture of multifold fermions at the R point also revealed Weyl spin–momentum locking. The discovery of Weyl spin–momentum locking may lead to energy-efficient memory devices and Josephson diodes based on chiral topological semimetals [5].

Controllable orbital angular momentum monopoles in chiral topological semimetals

The emerging field of orbitronics aims to generate and control electronic orbital angular momentum (OAM) currents for information processing. Topological crystals with structural chirality have been predicted to host topological band degeneracies in the reciprocal space, which are monopoles of the OAM; therefore, they could be particularly suitable orbitronic materials. Around such monopoles, the OAM is locked isotopically parallel or antiparallel to the direction of the electron momentum, which can be used to generate large and controllable OAM currents. However, OAM monopoles have not yet been directly observed in chiral crystals, and no means of controlling their polarity has been discovered. We used circular dichroism (CD)-ARPES to image OAM monopoles in the chiral topological semimetals PtGa and PdGa. Moreover, we demonstrated that the monopole polarity can be controlled via the structural handedness of the host crystal by imaging OAM monopoles and anti-monopoles in the two enantiomers of PdGa (Figure 5). For most photon energies used in our study, we observed a sign change in the CD-ARPES spectrum when comparing the positive and negative momenta along the light direction near the topological degeneracy. This is consistent with the conventional view that CD-ARPES measures the projection of OAM monopoles along the photon momentum direction. However, for some photon energies, this sign change disappears, which can be understood from our numerical simulations via the interference of polar atomic OAM contributions, which is consistent with the presence of OAM monopoles. Our results highlight the potential of chiral crystals for orbitronic devices. Moreover, our methodology should enable the discovery of even more complicated nodal OAM textures that can be exploited in orbitronics [6].

Chirality and superconductivity in $NbGe_2$

The interplay between topology and superconductivity in quantum materials harbors rich physical phenomena for discovery. We investigated the topological properties and superconductivity of the nonsymmorphic chiral superconductor $NbGe_2$ using high-resolution ARPES, transport measurements, and *ab initio* calculations. The ARPES data revealed exotic chiral surface states on the $NbGe_2$ (100) surface originating from the inherent chirality of the crystal structure. Supporting calculations indicate that $NbGe_2$ likely hosts elusive Weyl fermions in its bulk electronic structure. Furthermore, we uncovered signatures of van Hove singularities that can enhance many-body interactions. Additionally, our transport measurements demonstrated that $NbGe_2$ exhibits superconductivity below 2 K. Overall, our comprehensive results provide the first concrete evidence that $NbGe_2$ is a promising platform for investigating the interplay between nontrivial band topology, possible Weyl fermions, van Hove singularities, and superconductivity in chiral quantum materials (Figure 6).

Correlations and topology

The intersection of electronic topology and strong correlations offers a rich platform for discovering the exotic quantum phases of matter and unusual materials. An overarching challenge impeding these discoveries is the diagnosis of strongly correlated electronic topologies. We developed a framework to address this question and illustrate its power in determining the electronic topology of Mott insulators. Based on single-particle Green's functions, we introduced the concept of a frequency-dependent Green's function Berry curvature. We applied this notion to a system that contains symmetry-protected nodes in its noninteracting band structure. Strong correlations drive the system into a Mott-insulating state, creating contours in the frequency–momentum space where Green's function vanishes (Figure 7). The Green's function Berry flux of such zeros is quantized, and as such is a direct probe of the system's topology. Our framework allows for a systematic search of topological materials that are strongly correlated with Green's function topology [8].

Charge density waves in Kagome metals

Chiral transport signatures are allowed by symmetry in many conductors without a center of inversion; however, they only reach appreciable levels in rare cases with exceptionally strong chiral coupling to the itinerant electrons. So far, observations of chiral transport have been limited to materials in which the atomic positions strongly break the mirror symmetries. By contrast, we successfully observed chiral transport in the centrosymmetric layered kagome metal CsV_3Sb_5 (Figure 8) via second-harmonic generation under an in-plane magnetic field. The electronic magnetochiral anisotropy signal becomes significant only at temperatures below 35 K, deep within the charge-ordered state of CsV_3Sb_5 (charge density wave transition temperature $T_{CDW} \approx 94$ K). This temperature dependence reveals a direct correspondence between electronic chirality, unidirectional charge order [7], and spontaneous time-reversal symmetry breaking owing to putative orbital loop currents. We also showed that chirality is set by the out-of-plane field component and that a transition from left- to right-handed transport can be induced by changing the field sign. CsV_3Sb_5 is the first material in which strong chiral transport can be controlled and switched using small magnetic field changes – a prerequisite for applications in chiral electronics – in stark contrast to structurally chiral materials [9–11].

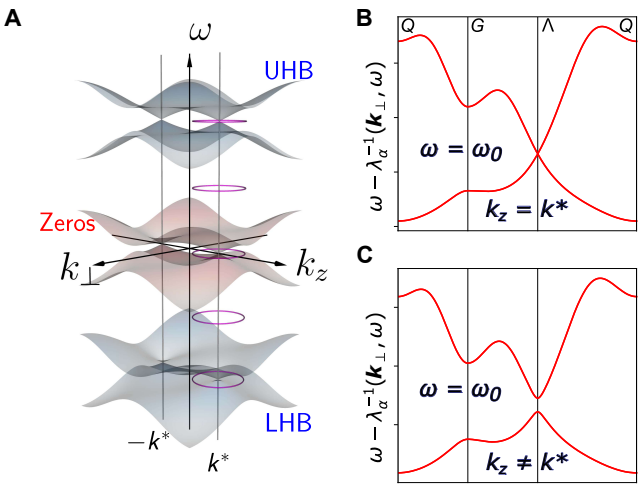

Fig. 7: Schematic plots of (a) retarded Green's function pole (red solid lines) and zero (green dashed lines) crossings as a function of k_z for a fixed (k_x, k_y). (b) $G + (k, \omega) - 1$ "bands" (or eigenvalues of $G + (k, \omega) - 1$) as a function of $k_\perp = (k_x, k_y)$ shifted by ω along high symmetry lines for a fixed ($k_z = k^*$, $\omega = \omega_0$). Λ, G, and Q are high-symmetry lines along the k_z direction, which become points for a fixed k_z.

Vision and perspective

Future research will focus on topological quantum chemistry to predict optimal materials for catalysis, including chiral surfaces and surface states, topological materials with spin–momentum locking for chiral electrons, and chiral phonons.

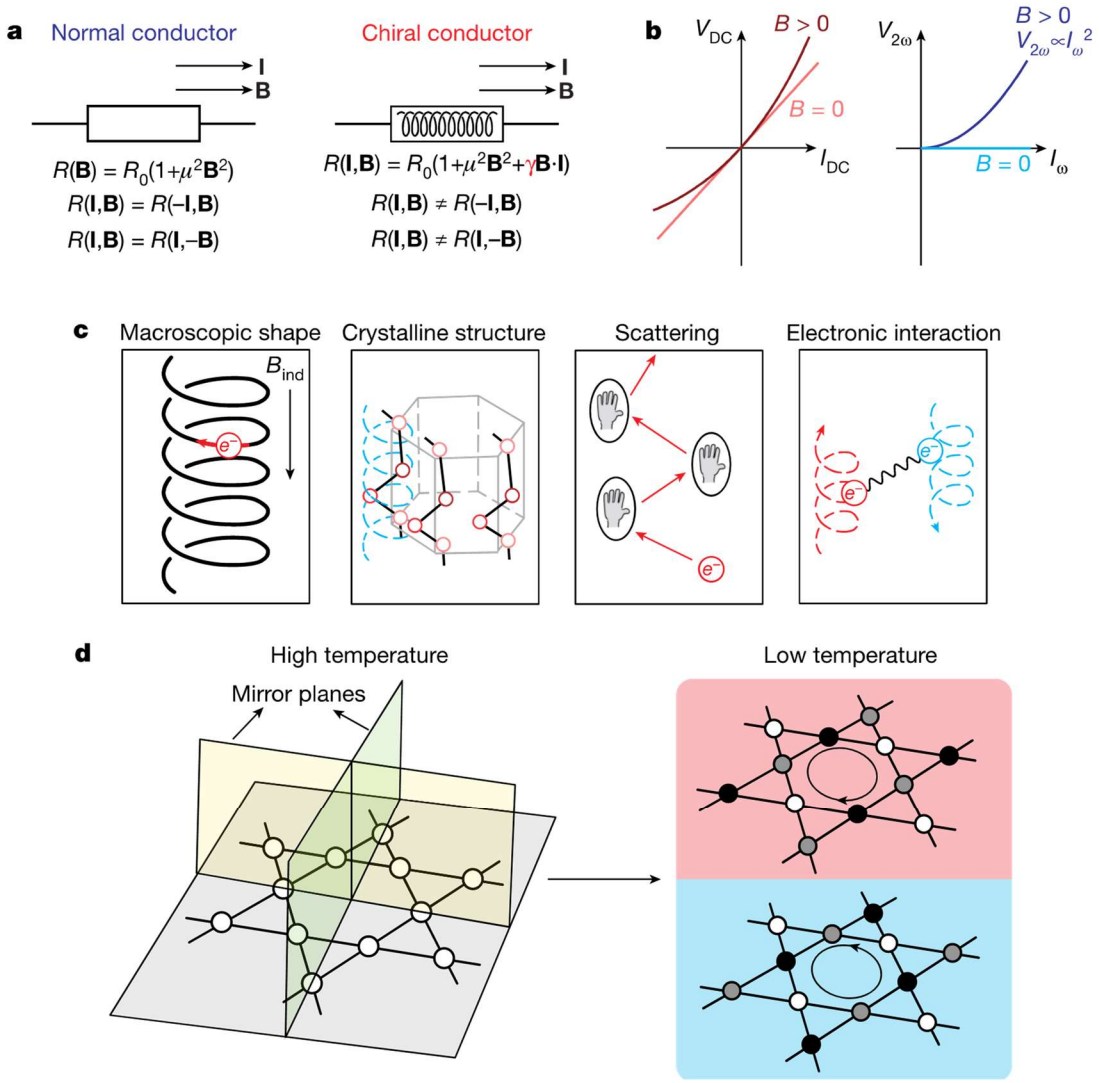

Fig. 8: Electronic magnetochiral anisotropy and spontaneous symmetry breaking in CsV_3Sb_5.

External Cooperation Partners

Qimiao Si (Rice University, USA); Martin Gutierrez-Amigo and Ion Errea (University of the Basque Country, Spain); Niels Schröter (MPI, Halle, Germany); Philip Moll (MPI, Hamburg, Germany).

References

[1]* *All topological bands of all nonmagnetic stoichiometric materials, M. G. Vergniory, B. J. Wieder, L. Elcoro, S. S. P. Parkin, C. Felser, B. A. Bernevig, N. Regnault, Science* ***20*** *(2022) 6595, https://doi.org/10.1126/science.abg9094*

[2]* *KMg_4Bi_3: A narrow band gap semiconductor with a channel structure, A. M. Ochs, D.-G. Oprea, J. Cardenas-Gamboa, C. E. Moore, J. P. Heremans, C. Felser, M. G Vergniory, J. E. Goldberger, Inorg Chem* ***63*** *(2024) 20133–20140, https://doi.org/10.1021/acs.inorgchem.4c00532*

[3]* *Catalogue of topological phonon materials, Y. Xu, M. G. Vergniory, D.-S. Ma, J. L. Mañes, Z.-D. Song, B. A. Bernevig, N. Regnault, L. Elcoro, Science* ***384*** *(2024), https://doi.org/10.1126/science.adf8458*

[4]* *Large anomalous Hall, Nernst effect and topological phases in the 3d-4d/5d-based oxide double perovskites, K. Samanta, J. Noky, I. Robredo, J. Kuebler, M. G. Vergniory, C. Felser, npj Comput Mater* ***9*** *(1) (2023) 167, https://doi.org/10.1038/s41524-023-01106-4*

[5]* *Weyl spin-momentum locking in a chiral topological semimetal, J. A. Krieger, S. Stolz, I. Robredo, K. Manna, E. C. McFarlane, M. Date, B. Pal, J. Yang, E. B. Guedes, J. H. Dil, C. M. Polley, M. Leandersson, C. Shekhar, H. Borrmann, Q. Yang, M. Lin, V. N. Strocov, M. Caputo, M. D. Watson, T. K. Kim, C. Cacho, F. Mazzola, J. Fujii, I. Vobornik, S. S. P. Parkin, B. Bradlyn, C. Felser, M. G. Vergniory, N. B. M. Schröter, Nat Commun* ***15*** *(1) (2024) 3720, https://doi.org/10.1038/s41467-024-47976-0*

[6] *Controllable orbital angular momentum monopoles in chiral topological semimetals, Y. Yen, J. A. Krieger, M. Yao, I. Robredo, K. Manna, Q. Yang, E. C. McFarlane, C. Shekhar, H. Borrmann, S. Stolz, R. Widmer, O. Gröning, V. N. Strocov, S. S. P. Parkin, C. Felser, M. G. Vergniory, M. Schüler, N. Schröter, Nat Phys (2024), https://doi.org/10.1038/s41567-024-02655-1*

[7] *Observation of chiral surface state in superconducting $NbGe_2$, M. Yao, M. Guierrez-Amigo, S. Roychowdhury, I. Errea, A. Fedorov, V. N. Strocov, M. G. Vergniory, C. Felser, under review in Nat Commun. Preprint: https://doi.org/10.48550/arXiv.2403.03324*

[8] *Topological diagnosis of strongly correlated electron systems, C. Setty, F. Xie, S. Sur, L. Chen, S. Paschen, M. G. Vergniory, J. Cano, Q. Si, under review in Sci Adv. Preprint: https://doi.org/10.48550/arXiv.2311.12031*

[9]* *Switchable chiral transport in charge-ordered kagome metal CsV_3Sb_5, C. Guo, C. Putzke, S. Konyzheva, X. Huang, M. Gutierrez-Amigo, I. Errea, D. Chen, M. G. Vergniory, C. Felser, M. H. Fischer, T. Neupert, P. J. W. Moll, Nature **611** (7936) (2022) 461–466, https://doi.org/10.1038/s41586-022-05127-9*

[10]* *Correlated order at the tipping point in the kagome metal CsV_3Sb_5, C. Guo, G. Wagner, C. Putzke, D. Chen, K. Wang, L. Zhang, M. Gutierrez-Amigo, I. Errea, M. G. Vergniory, C. Felser, M. H. Fischer, T. Neupert, P. J. W. Moll, Nat Phys **20** (2024) 579–584, https://doi.org/10.1038/s41567-023-02374-z*

[11]* *Three-dimensional Fermi surfaces from charge order in layered CsV_3Sb_5, X. Huang, C. Guo, C. Putzke, M. Gutierrez-Amigo, Y. Sun, M. G. Vergniory, I. Errea, D. Chen, C. Felser, P. J. W. Moll, Phys Rev B **106** (6) (2022) 064510, https://doi.org/10.1103/PhysRevB.106.064510*

[#]maia.vergniory@cpfs.mpg.de
[##]claudia.felser@cpfs.mpg.de